OPTIMIZATION WITH THE PETRA IV LATTICE SEXTUPOLES FOR THE MITIGATION OF MAGNETIC FIELD IMPERFECTIONS

K. Paraschou*, I. Agapov, A. Aloev, R. Bartolini, E. Musa
Deutsches Elektronen-Synchrotron DESY, Hamburg, Germany

Abstract

As is typical for the design of a fourth-generation light source, PETRA IV includes strong quadrupolar and sextupolar magnets, making the beam dynamics of the storage ring sensitive to magnetic field imperfections. In particular, we show that field imperfections in the quadrupoles can drive nonlinear resonances which can limit the efficiency of the top-up injection scheme in PETRA IV through a reduction of dynamic aperture. This work explores different operational strategies for modifying the strengths of the sextupolar magnets to recover a potential loss in the dynamic aperture and injection efficiency.

INTRODUCTION

The PETRA IV storage ring [1–3] is planned to operate continuously with off-axis top-up injection to recover the charge lost in the beam. It is therefore crucial to have sufficient dynamic aperture in order not to degrade injection efficiency. In PETRA IV, the dynamic aperture is significantly affected by betatron resonances. In particular, the half-integer resonance is known to strongly reduce the dynamic aperture in the horizontal plane with realistic residual linear optics errors.

Normal sextupolar errors, either due to multipolar imperfections in the quadrupole magnets or due to field errors in the sextupole magnets, can excite the third-order resonances $3Q_x, Q_x - 2Q_y$. Correction of such errors in simulations is the subject of this contribution. These errors are expected to arise from the finite precision in aligning the magnet poles. Errors under realistic alignment tolerances are enough to excite the aforementioned third-order resonances and degrade the dynamic aperture down to 5 mm. The dynamic aperture for 100 random realizations of the lattice with residual linear optics errors is visible in Fig. 1. The dynamic aperture after introducing normal sextupole errors (10 b_3 units) is shown in Fig. 2. From the comparison of the two, the dynamic aperture can go from 7-10 mm down to 5 mm. It is clear that with errors of this magnitude, the injection efficiency will get strongly affected as the injected beam (dashed line) overlaps the dynamic aperture.

It is important to note that the quality of the PETRA IV quadrupoles to be procured must meet stricter specifications in order to minimize the risk of operating with suboptimal injection efficiency. Nevertheless, mitigation measures are presented here to alleviate the effects of possible unaccounted b_3 errors. All presented correction strategies use all of the 432 individually powered sextupoles in the PETRA IV lattice.

* konstantinos.paraschou@desy.de

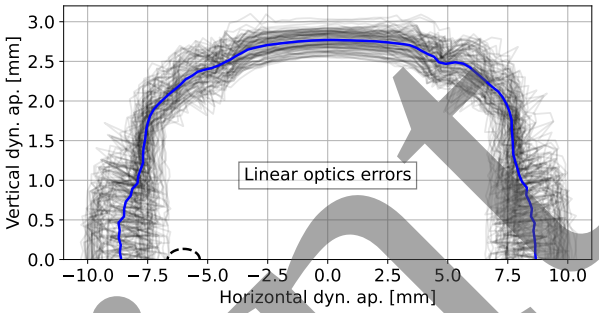

Figure 1: Dynamic aperture with simplified linear optics errors in the PETRA IV lattice, evaluated over 100 error seeds. The dashed line depicts the position and r.m.s. beam size of the injected beam.

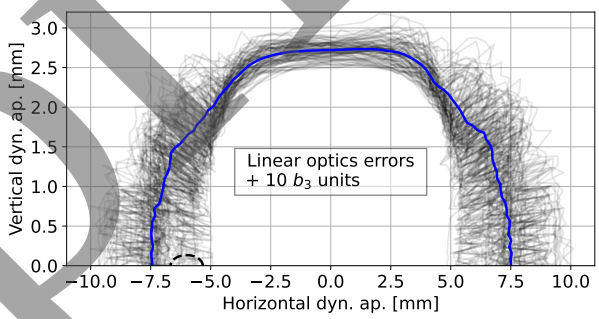

Figure 2: Dynamic aperture with simplified linear optics and b_3 errors in the PETRA IV lattice, evaluated over 100 error seeds. The dashed line depicts the position and r.m.s. beam size of the injected beam.

For this contribution, a simplified scenario is considered where approximately 3 % r.m.s. beta-beating is introduced by assigning a 0.05 % relative field error on all quadrupoles. The dynamic aperture of the 100 random seeds of the lattice is shown in Fig. 1. The dynamic aperture throughout the study is evaluated at the injection point with the Accelerator Toolbox [4,5] tracking code, including the model of physical apertures in the simulation. In this study, it is assumed that the DESY IV booster will serve as the injector of PETRA IV. The r.m.s. beam size contour is drawn in Fig. 1. For the optimization studies, the injected beam is assumed to be injected close to the dynamic aperture with a −6 mm offset with respect to the stored beam, instead of assuming a more optimal injection offset in terms of injection efficiency. The b_3 imperfection (normal sextupole) of a quadrupole is sampled from a random normal distribution with a standard deviation equal to 10 “magnet units” (at a reference radius of 6.5 mm) [6].

IDEAL CORRECTION

Normal sextupole errors manifest primarily in a change of off-momentum linear optics functions, i.e. off-momentum betatron functions, chromatic phase advances and Montague chromatic amplitudes [7], all of which are interrelated. Additionally, they produce geometric aberrations in the transverse phase space of even on-momentum particles. These are frequently quantified in terms of the complex-valued Resonance Driving Term (RDT) functions [8]. Particularly relevant are the RDT functions f_{3000} and f_{1002} which are associated with the $3Q_x$ and $Q_x - 2Q_y$ resonances, respectively. An ideal correction of these errors can be performed by inverting the following matrix equation. It expresses the change of the real and imaginary parts of the RDTs f_{3000},f_{1002} and horizontal and vertical phase advances $\partial\mu_x/\partial\delta$, $\partial\mu_y/\partial\delta$, when there is a change in the normalized strength of the sextupoles.

$$\begin{pmatrix} \Re[\vec{f}_{3000}] \\ \Im[\vec{f}_{3000}] \\ \Re[\vec{f}_{1002}] \\ \Im[\vec{f}_{1002}] \\ \partial\vec{\mu}_x/\partial\delta \\ \partial\vec{\mu}_y/\partial\delta \end{pmatrix} - \begin{pmatrix} \Re[\vec{f}^{\,0}_{3000}] \\ \Im[\vec{f}^{\,0}_{3000}] \\ \Re[\vec{f}^{\,0}_{1002}] \\ \Im[\vec{f}^{\,0}_{1002}] \\ \partial\vec{\mu}_x{}^{0}/\partial\delta \\ \partial\vec{\mu}_y{}^{0}/\partial\delta \end{pmatrix} = \mathbf{R} \cdot \begin{pmatrix} \Delta k_{2,1} \\ \Delta k_{2,2} \\ \Delta k_{2,3} \\ \Delta k_{2,4} \\ \vdots \\ \Delta k_{2,N} \end{pmatrix}. \quad (1)$$

In the left-hand side of Eq. (1), the observables are calculated at each beam position monitor location. The difference of their values with respect to those in the design lattice f^0_{3000},f^0_{1002}, $\partial\mu^0_x/\partial\delta$, and $\partial\mu^0_y/\partial\delta$ is evaluated and serves as the objective to minimize. The total number amounts to 6 observables for each of the 786 beam position monitors. In the right-hand side, the matrix $\mathbf{R}$ (of size 4716×432) contains the response of these quantities with respect to a change in the normalized strength of the i^{th} sextupole $\Delta k_{2,i}$. Given a set of measurements of the above quantities, a least-squares solution can be obtained by computing the pseudo-inverse of $\mathbf{R}$ with the singular value decomposition algorithm and an appropriate truncation of the singular value spectrum.

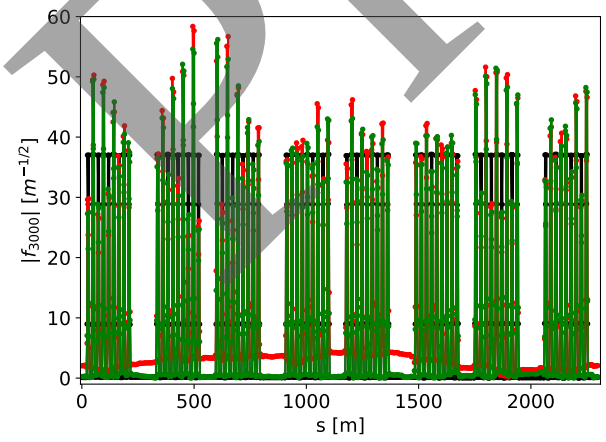

Figure 3: Resonance driving term f_{3000} function in the (black) design lattice, (red) lattice with linear optics and b_3 errors and (green) after response matrix correction.

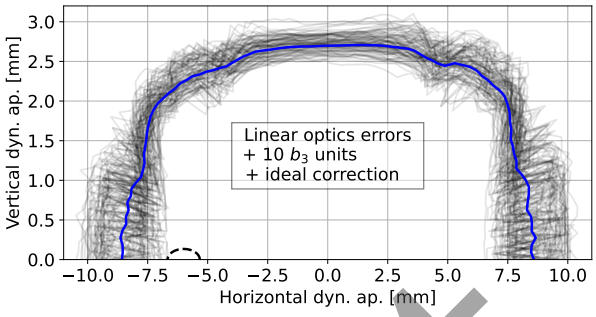

Figure 4: Dynamic aperture with simplified linear optics, b_3 errors in the PETRA IV lattice, and after idealized sextupole corrections, evaluated over 100 error seeds. The dashed line depicts the position and r.m.s. beam size of the injected beam.

These observables can be easily calculated with tracking codes in simulations. However, their experimental measurement is not trivial. Although they have been successfully measured in third-generation light sources with turn-by-turn methods [8], fourth-generation light sources exhibit much stronger nonlinearities which may severely limit their effectiveness. Nevertheless, even if the above quantities are not practically measurable, a correction based on them is a good benchmark on the level of correction that can be achieved.

By applying this correction to one of the seeds showing a significant dynamic aperture degradation from before, the residual RDT terms are minimized. An example of the magnitude of $f_{3000}(s)$ is shown in Fig. 3. The pattern in the RDT is characteristic of a hybrid multi-bend achromat that uses a $-\mathbf{I}$ transform between sets of sextupoles to locally cancel the RDTs. As a result, in the design lattice (black) the RDT assumes a large value between pairs of sextupoles, and a small "baseline" between the cells. The sextupole errors have the effect of visibly increasing the "baseline" (red). As expected, the "baseline" is restored after the correction (green).

This ideal correction procedure is then applied to the set of random errors described in the previous section. The correction converges within 5 iterations. The result of the dynamic aperture over all 100 random lattices is presented in Fig. 4. The dynamic aperture is fully recovered when comparing both the worst-performing seeds and the average dynamic aperture in Fig. 1. However, the measurements required to perform this correction might not be feasible.

BAYESIAN OPTIMIZATION

In order to overcome the likely limitation of not having a good enough measurement of the required RDT observables, a reduced set of knobs is developed. Then, injection efficiency is used as the objective to maximize, as it is a readily available observable. A similar strategy is routinely employed in the ESRF-EBS light source [9, 10], where the Badger and Xopt [11–13] software libraries are used to perform Bayesian optimization by maximizing either injection efficiency or beam lifetime. In their case, several knobs were

tested based on eigenvector analysis of the derivative of an orbit response matrix and on sinusoidal patterns around the ring, and optimized by observing beam lifetime.

Given the direct link between the resonance excitation and the degradation of dynamic aperture for the case of PETRA IV, knobs based on RDTs are studied here. In the first case, four knobs are designed based on the response of the real and imaginary parts of f_{3000} and f_{1002}, evaluated only at the start of the lattice $s = 0$, and the change in linear horizontal and vertical chromaticity Q'_x, Q'_y. This leads to a matrix equation in the form of:

$$\begin{pmatrix} \Re[f_{3000}(0)] \\ \Im[f_{3000}(0)] \\ \Re[f_{1002}(0)] \\ \Im[f_{1002}(0)] \\ Q'_x \\ Q'_y \end{pmatrix} - \begin{pmatrix} \Re[f^0_{3000}(0)] \\ \Im[f^0_{3000}(0)] \\ \Re[f^0_{1002}(0)] \\ \Im[f^0_{1002}(0)] \\ Q'^0_x \\ Q'^0_y \end{pmatrix} = \mathbf{M} \cdot \begin{pmatrix} \Delta k_{2,1} \\ \Delta k_{2,2} \\ \Delta k_{2,3} \\ \Delta k_{2,4} \\ \vdots \\ \Delta k_{2,N} \end{pmatrix}. \quad (2)$$

Here, $\mathbf{M}$ (of size 6×432) can be calculated in the design lattice and its pseudo-inverse can be calculated once more with singular value decomposition. The rows of the pseudo-inverse matrix will provide directly 6 independent sextupole knobs, each affecting exclusively the specific observable. The 4 knobs affecting the RDTs are used as variables with the Trust Region Bayesian Optimization (TuRBO) algorithm implemented in Xopt [12, 14]. Simulations of injection efficiency are used as the target to optimize. The two chromaticity knobs are held fixed to keep the linear chromaticities constant. The procedure is applied on the same random lattices that were studied in the previous section. The optimization is run over 50 steps. An example of the evolution of injection efficiency for one of the seeds is visible in Fig. 5, where the optimizer converges in a small number of steps.

The resulting dynamic aperture for all 100 random lattices is reported in the top panel of Fig. 6. The optimization based on the 4 knobs is very effective at recovering the dynamic aperture in the worst performing seeds. On the other hand, the improvement is not as good when comparing the average dynamic apertures. Given the limited number of knobs

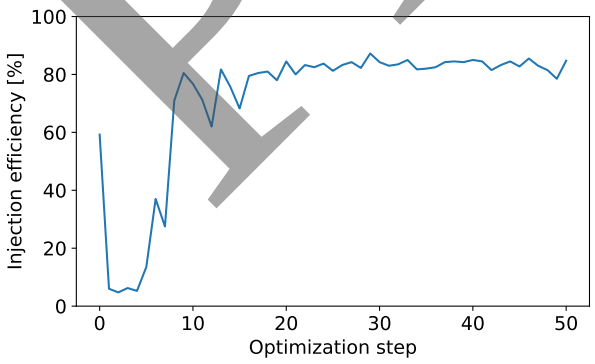

Figure 5: Example evolution of injection efficiency during its optimization using the 4 simplified knobs, in one of the random lattices.

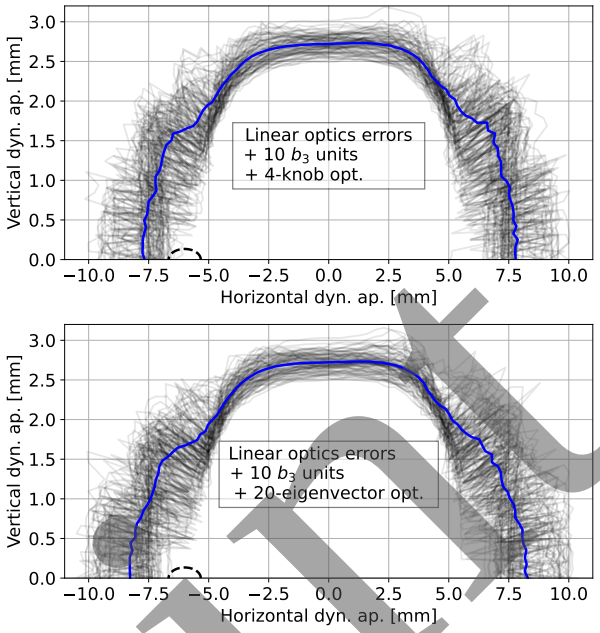

Figure 6: Dynamic aperture with simplified linear optics, b_3 errors in the PETRA IV lattice, and after Bayesian optimization with (top) 4 knobs and (bottom) 20 eigenvectors, evaluated over 100 error seeds. The dashed line depicts the position and r.m.s. beam size of the injected beam.

required, the method serves as a good compromise for rough targeted optimizations.

A more brute-force approach uses the same Bayesian optimization algorithm but instead uses the first N eigenvectors of the response matrix $\mathbf{R}$ defined in Eq. (1). The example of using the first 20 eigenvectors as knobs is presented in the bottom panel of Fig. 6. The optimization is efficient at recovering both the average dynamic aperture as well as the dynamic aperture of the worst performing seeds, at the cost of a considerably larger number of dimensions.

CONCLUSION

Quadrupole field imperfections in PETRA IV can drive third-order resonance terms and reduce the DA available for top-up injection. The studies presented here compare three sextupole-based mitigation strategies using DA calculations over 100 error seeds. The ideal correction of f_{3000}, f_{1002}, and chromatic phase-advance functions gives the best recovery and therefore defines the reference performance of the available sextupole degrees of freedom. The two Bayesian optimization strategies provide more operationally practical alternatives. The four-knob method has a small search space tied directly to a global RDT response, while the 20-eigenvector method includes additional local (s-dependent) information through the full response matrix. Both approaches are expected to recover only part of the ideal correction performance, but they reduce the reliance on difficult direct measurements of the full nonlinear correction target.

REFERENCES

[1] C. G. Schroer *et al.*, *PETRA IV: upgrade of PETRA III to the ultimate 3d x-ray microscope. conceptual design report*. Hamburg, Germany: Deutsches Elektronen-Synchrotron DESY, 2019. doi:10.3204/PUBDB-2019-03613

[2] I. Agapov *et al.*, "Beam dynamics performance of the proposed PETRA IV storage ring", 2024, arXiv: 2408.07995 [physics.acc-ph],

[3] R. Bartolini *et al.*, "Status of the PETRA IV accelerators upgrade", presented at the 17th International Particle Accelerator Conf. (IPAC'26), Deauville, France, May 2026, paper THV2001, this conference.

[4] A. Terebilo, "Accelerator toolbox for matlab", SLAC National Accelerator Laboratory, Rep. SLAC-PUB-8732, 2001. doi:10.2172/784910

[5] W. A. H. Rogers, N. Carmignani, L. Farvacque, and B. Nash, "Pyat: a python build of accelerator toolbox", in *Proc. IPAC'17*, pp. 3855–3858, 2017. doi:10.18429/JACoW-IPAC2017-THPAB060

[6] *Handbook of Accelerator Physics and Engineering*, A. W. Chao, M. Tigner, H. Weise, and F. Zimmermann, Eds. Singapore: World Scientific, 2023. doi:10.1142/13229

[7] B. W. Montague, "Linear optics for improved chromaticity correction", CERN, Geneva, Switzerland, Rep. CERN-LEP-Note-165, 1979. cds.cern.ch/record/443342

[8] A. Franchi, L. Farvacque, F. Ewald, G. L. Bec, and K. B. Scheidt, "First simultaneous measurement of sextupolar and octupolar resonance driving terms in a circular accelerator from turn-by-turn beam position monitor data", *Phys. Rev. Spec. Top. Accel. Beams*, vol. 17, p. 074001, 2014. doi:10.1103/PhysRevSTAB.17.074001

[9] P. Raimondi *et al.*, "Commissioning of the hybrid multibend achromat lattice at the European Synchrotron Radiation Facility", *Phys. Rev. Accel. Beams*, vol. 24, p. 110701, 2021. doi:10.1103/PhysRevAccelBeams.24.110701

[10] P. Raimondi *et al.*, "The extremely brilliant source storage ring of the European Synchrotron Radiation Facility", *Commun. Phys.*, vol. 6, p. 82, 2023. doi:10.1038/s42005-023-01195-z

[11] Z. Zhang *et al.*, "Badger: the missing optimizer in ACR", in *Proc. IPAC'22*, Bangkok, Thailand, pp. 999–1002, 2022. doi:10.18429/JACoW-IPAC2022-TUPOST058

[12] R. Roussel, C. Mayes, A. Edelen, and A. Bartnik, "Xopt: a simplified framework for optimization of accelerator problems using advanced algorithms", in *Proc. IPAC'23*, Venice, Italy, May 2023, pp. 4847–4850. doi:10.18429/JACoW-IPAC2023-THPL164

[13] S. M. Liuzzo *et al.*, "Optimisation of the touschek lifetime in synchrotron light sources using badger", in *Proc. 19th Int. Conf. Accel. Large Exp. Phys. Control Syst. (ICALEPCS'23)*, Cape Town, South Africa, Oct. 2023, pp. 108–115. doi:10.18429/JACoW-ICALEPCS2023-MO3AO01

[14] D. Eriksson, M. Pearce, J. Gardner, R. D. Turner, and M. Poloczek, "Scalable global optimization via local bayesian optimization", in *Proc. Conf. Adv. Neural Inf. Process. Syst. (NeurIPS'19)*, Vancouver, BC, Canada, Dec. 2019, pp. 5497–5508.